Polymer Journal (2017) 49, 215–221

www.nature.com/pj

ORIGINAL ARTICLE

Alkylated oxygen-bridged V-shaped molecules: impacts of the substitution position and length of the alkyl chains on the crystal structures and fundamental properties in aggregated forms

Chikahiko Mitsui[1,2], Tatsuro Annaka[1], Ken-ichi Nakamura[1], Masato Mitani[1,2], Daisuke Hashizume[2], Katsumasa Nakahara[1], Masakazu Yamagishi[1], Takanari Ueno[3], Yuji Tanaka[3], Masafumi Yano[3], Daichi Iwasawa[4], Miki Hasegawa[4], Hiroyasu Sato[5], Akihito Yamano[5], Jun Takeya[1] and Toshihiro Okamoto[1,2,6]

We have recently developed dinaphtho[2,3-*b*:2',3'-*d*]furan (DNF–V) derivatives as a new type of solution-processable organic semiconducting material with high carrier mobility and high emission efficiency in the solid state. In this article, we systematically investigate and reveal the impact of the substitution position and the length of the alkyl side chains on their physicochemical properties based on their packing structures. For both alkylated DNF–VV and DNF–VW derivatives, the solubilities and the phase-transition temperatures increase as the shorter alkyl chains are attached. In particular, alkylated DNF–VV simultaneously achieve high solubility (over 1 wt%) and a highly stabilized crystal phase (up to 199 °C). Furthermore, DNF–V derivatives exhibit a deep-blue emission in the solid state with a quantum efficiency ranging from 17 to 51%. Such a range of physicochemical properties is probably related to the dependencies on the molecular geometry in the crystal state and the length of the alkyl side chains.
Polymer Journal (2017) **49,** 215–221; doi:10.1038/pj.2016.105; published online 9 November 2016

INTRODUCTION

The functionality of π-conjugated organic materials is determined by rational molecular design. The primary strategy in the design of organic semiconductor materials relies on π-electron systems composed of benzene- and/or heterole-fused π-electronic cores, which play an essential role in organic field-effect transistors.[1] One of the most important advantages and requirements of organic field-effect transistors is the low-cost device fabrication enabled by the solution processability of the organic semiconductor materials. For the applications of such organic materials to driving circuits of displays and radio frequency identifier tags,[2,3] the development of solution-processable high-mobility organic semiconductors is a crucial issue. Historically, pentacene has been regarded as a benchmark of high-performance organic semiconductors,[4] and its derivatives have been extensively developed.[5,6] The fatal drawbacks of pentacene (that is, its chemical instability and low solubility) were overcome by structural modification; for example, introduction of triisopropylsilylethynyl groups at 6,13-positions.[5,7] While triisopropylsilylethynyl pentacene shows chemical stability and improved solubility together with high carrier mobility in solution-processed film[8,9] exceeding that of amorphous silicon (0.5–1.0 $cm^2\ V^{-1}\ s^{-1}$), it transforms into the liquid crystal phase at 124 °C.[10] Therefore, the development of practically applicable organic semiconductors featuring solution processability and a thermally stable aggregated form that enables device thermal durability is a particular challenge because these features are often in a trade-off relationship.[10–12] To address this formidable challenge, we recently developed bent-shaped π-electronic cores with oxygen and sulfur-bridged V-shaped π-conjugated molecules, dinaphtho[2,3-*b*:2′,3′-*d*]chalcogenophene (**DNF–V** and **DNT–V**, Figure 1).[13,14] Alkylated V-shaped molecules possess solution-processability and moderately high structural stability in the crystal phase and exhibit high carrier mobility over 1.0 $cm^2\ V^{-1}\ s^{-1}$. Notably, the bridged chalcogen atoms have a significant impact on the electronic properties and aggregate structures. In particular, because of the light oxygen atom, **DNF–V** exhibits a deep blue-emission with a high quantum yield of 72% in the solid state, while the sulfur-bridged congener, **DNT–V**, exhibits almost no emission. The **DNF–V** based organic semiconductor with high carrier mobility and a high luminescence property could be a promising candidate for organic light-emitting transistors.[15] In this article, we systematically

[1]Department of Advanced Materials Science, Graduate School of Frontier Sciences, The University of Tokyo, Chiba, Japan; [2]Materials Characterization Support Unit, Center for Emergent Matter Science (CEMS), Saitama, Japan; [3]Chemistry, Materials and Bioengineering Major, Graduate School of Science and Engineering, Kansai University, Osaka, Japan; [4]Department of Chemistry and Biological Science, College of Science and Engineering, Aoyama Gakuin University, Kanagawa, Japan; [5]Rigaku Corporation, Tokyo, Japan and [6]PRESTO, Japan Science and Technology Agency (JST), Saitama, Japan
Correspondence: Professor T Okamoto, Department of Advanced Materials Science, The University of Tokyo, 5-1-5 Kashiwanoha, Kashiwa, Chiba 277-8561, Japan.
E-mail: tokamoto@k.u-tokyo.ac.jp
Received 30 June 2016; revised 18 September 2016; accepted 20 September 2016; published online 9 November 2016

investigate alkylated **DNF–V** derivatives (*herein* referred to for 3,9-substitution as **C$_n$–DNF–VW**s and for 2,10-substitution as **C$_n$–DNF–VV**s) and shed light on the impact of the substitution position and the length of the alkyl side chains on their physicochemical properties and packing structures, solubilities, thermal properties and photophysical properties. Intriguingly, as the shorter alkyl chains are substituted on the **C$_n$–DNF–VV**s, these molecules possess a higher solubility of over 1.0 wt% and a higher phase-transition temperature of ~ 200 °C. This trend is conducive to producing semiconductor materials with solution-processability and thermal durability. This investigation provides us a rational molecular design for the development of practical organic semiconducting materials.

MATERIALS AND METHODS

All the reactions were performed under an atmosphere of nitrogen. Air- or moisture-sensitive liquids and solutions were transferred via a syringe or a Teflon cannula. General synthesis procedures for each step are described in the Supplementary Information. Analytical thin-layer chromatography was performed on glass plates with 0.25 mm 230–400 mesh silica gel containing a fluorescent indicator (Silica gel 60 F254, Merck Millipore Corporation). The thin-layer chromatography plates were visualized via exposure to an ultraviolet lamp (254 and 365 nm), followed by dipping with 10% phosphomolybdic acid in ethanol and heating on a hot plate. Flash column chromatography was performed on Kanto silica gel 60. Open column chromatography was performed on Wakogel C-200 (75–150 μm). All NMR spectra were recorded using JEOL ECA600 and JEOL ECS400 spectrometers. Mass spectra were measured using a JEOL JMS-T100LC APCI/ESI mass spectrometer. Melting points and elemental analyzes were collected using a Mettler Toledo MP70 Melting Point System and a J-Science Lab JM10 MICRO CORDER, respectively. Thermogravimetric analysis measurements were performed using a Rigaku Thermo Plus EVO II TG 8120. Each sample was placed in an aluminum pan and then heated at the rate of 5 K min^{-1} under N_2 purge at a flow rate of 100 ml min^{-1}. Al_2O_3 was used as a reference material. Differential scanning calorimetry (DSC) measurements were performed using a Rigaku Thermo Plus EVO II DSC8270. Each sample was placed in an aluminum pan and then heated at the rate of 5 K min^{-1} under N_2 purge at a flow rate of 100 ml min^{-1}. Al_2O_3 was used as a reference material. Ultraviolet–vis absorption spectra were measured using a JASCO V-570 spectrometer. Thin films with a thickness of 100 nm on quartz substrates were prepared using vacuum deposition. The samples in solutions were prepared in degassed and analytical grade 1,2-dichloroethane. Photoluminescence spectra and absolute quantum yields were recorded using a Hamamatsu Photonics C9920-02 Absolute PL Quantum Yield Measurement System. The samples in solution were prepared in degassed and analytical grade 1,2-dichloroethane. Fluorescence lifetimes were evaluated with a Hamamatsu Photonics Quantaurus-Tau C11367-01 measurement system. The excitation spectrum monitored at each fluorescence band position well corresponds to the electronic absorption spectrum.

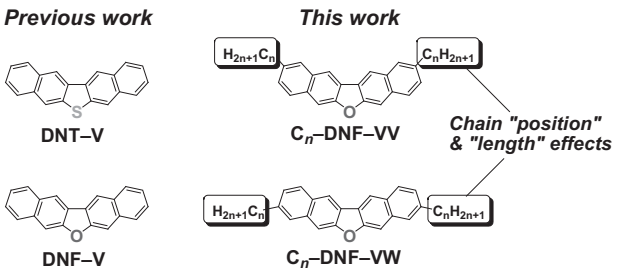

Figure 1 Chemical structures of the **DNT–V** and **DNF–V** derivatives. A full color version of this figure is available at *Polymer Journal* online.

RESULTS AND DISCUSSION

Synthesis

Previously, we developed a facile and cost-effective synthetic protocol for constructing the **DNF–V** framework. Applying this synthetic method, we newly synthesized **DNF–V** derivatives with hexyl and octyl groups at the 3,9- and 2,10-positions, respectively, as shown in Scheme 1. Starting from either 2-alkyl-7-methoxynaphthalene or 2-alkyl-6-methoxynaphthalene, the homo-coupling proceeded smoothly *via ortho*-lithiation with *n*-butyllithium followed by

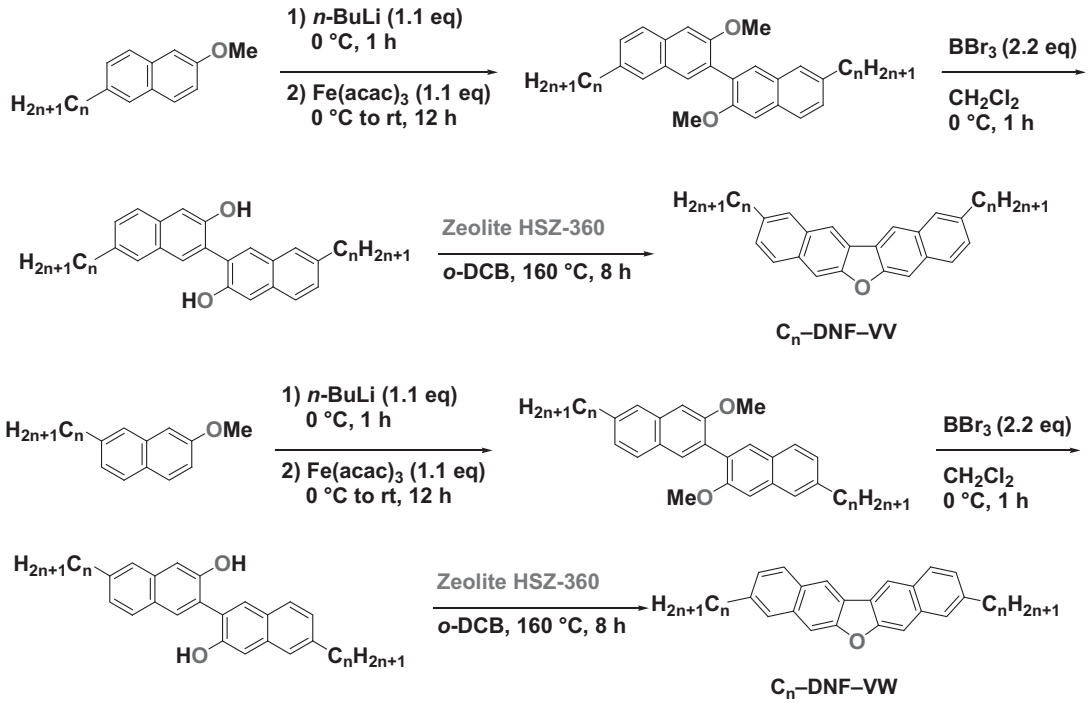

Scheme 1 Facile synthetic route of alkylated **DNF–V** derivatives. A full color version of this scheme is available at *Polymer Journal* online.

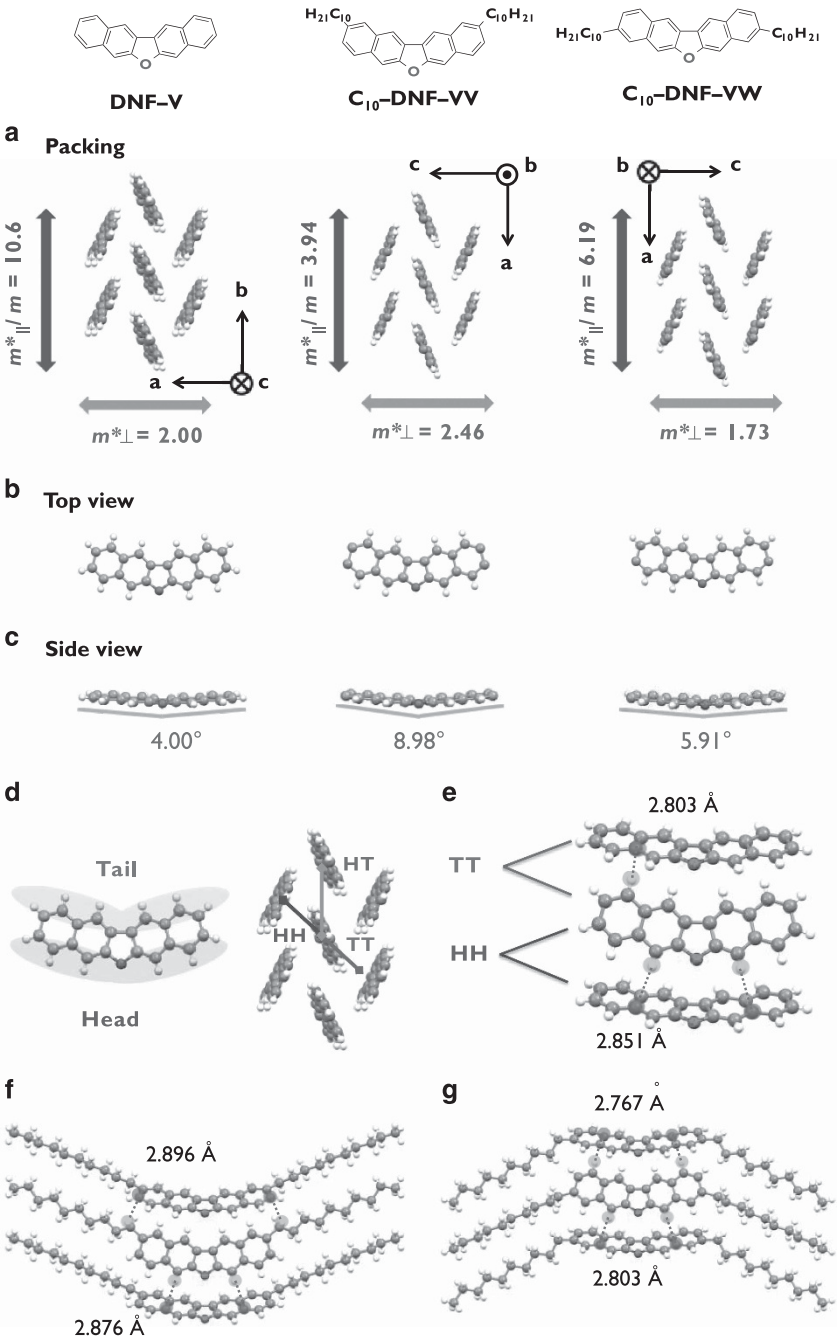

Figure 2 Packing structures (**a**) and front (**b**) and side views together with dihedral angles (**c**) of **DNF–V**, **C_{10}–DNF–VV**, and **C_{10}–DNF–VW**. Definition of the 'Head (H)' and 'Tail (T)' of **DNF–V** core (**d**). Neighboring intermolecular short contacts of **DNF–V**s (**e**–**g**). The decyl groups are omitted for clarity. A full color version of this figure is available at *Polymer Journal* online.

oxidation using an iron (III) reagent. Subsequent demethylation afforded 2,2′-binaphthalene diols as the key precursors. Finally, on treatment with a zeolite catalyst, dehydration proceeded to afford **DNF–V** derivatives in an almost quantitative yield. In this synthetic methodology, the overall yields of alkyl substituted **DNF–V**s, regardless of the positions and lengths of the alkyl chains, were 40–67%.[16]

Single crystal structure analysis

Using the crystal structures of **DNF–V** derivatives reported previously,[14] we discuss the packing structures and their carrier transporting abilities more in detail. Note that **DNF–V** derivatives assemble in herringbone packing motifs and their core structures are slightly bent, with the dihedral angle of 4.00–8.98° between two naphthalene units in a single crystal, as illustrated in Figure 2a–c. Such bent structures are contrary to the results of the theoretical calculation, in which the optimized **DNF–V** geometries are completely planar. Such a distorted structure in the single crystal can be understood by the characteristics of V-shaped molecules assembling in the herringbone packing. In this packing mode, the **DNF–V** core affects the planarity of neighboring **DNF–V** molecules in head-to-head and tail-to-tail fashions. Here, we define the 'head' as a side of the prominent oxygen atom of the **DNF–V** core and the 'tail' as the opposite side of

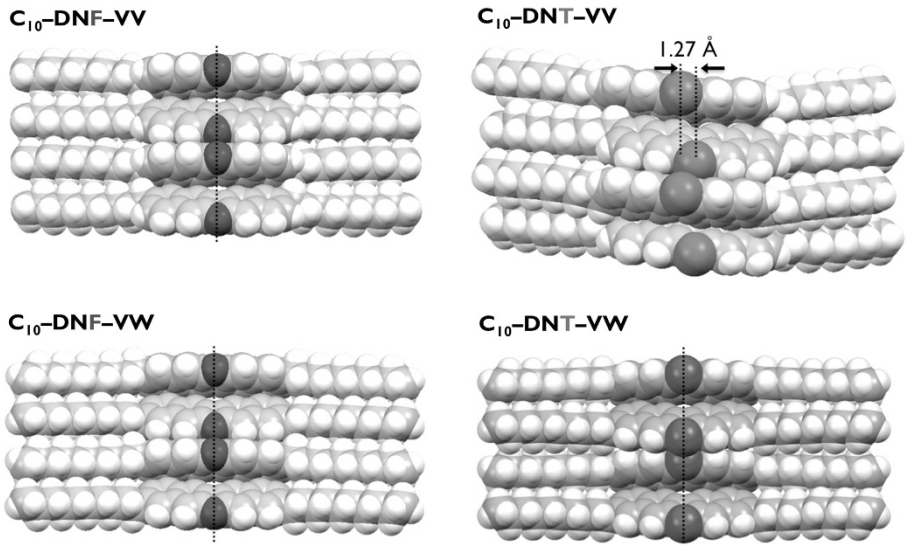

Figure 3 Packing structures and molecular displacements of the **C_{10}–DNF–V** and **C_{10}–DNT–V** derivatives. A full color version of this figure is available at *Polymer Journal* online.

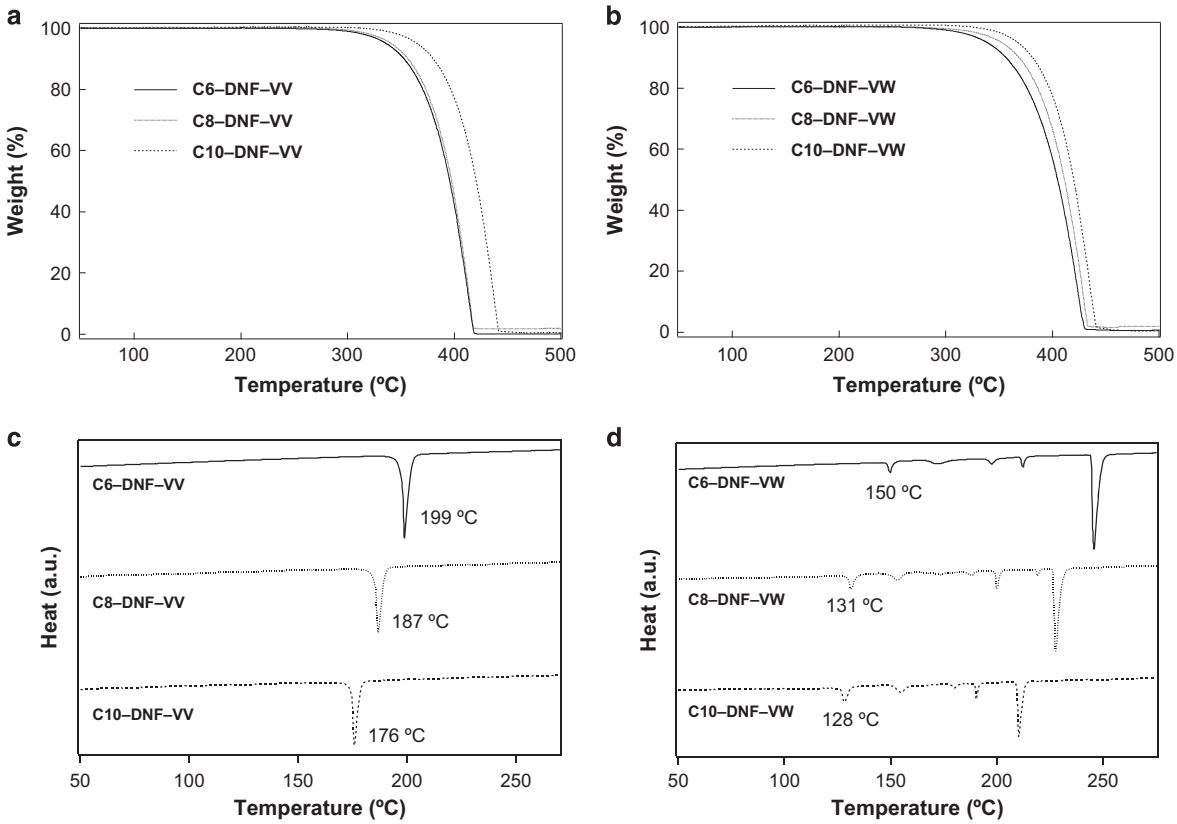

Figure 4 Thermogravimetric analysis charts of **C_n–DNF–VV** (**a**) and **C_n–DNF–VW** (**b**). DSC traces of **C_n–DNF–VV** (**c**) and **C_n–DNF–VW** (**d**).

the molecule, as depicted in Figure 2d. When the **DNF–V** cores deform out of plane, they interact with both the head and the tail molecules more effectively via attractive intermolecular interaction, such as van der Waals forces and C-H···π interactions, which are observed as short contacts (Figure 2e–g). Such stabilization energy could offset the destabilization energy resulting from the deviation of the planarity. The molecular geometries are, therefore, transformed into the non-planar structures and the adjacent molecules. In comparison with the parent **DNF–V** and **C_n–DNF–VW**s, the structure of **C_{10}–DNF–VV** is much more non-planar, with a dihedral angle of 8.98°. As depicted in Figure 2f, the interaction between the outer benzene rings and the protons at the benzyl positions of the alkyl chains were observed; this interaction might induce a more bent conformation. With respect to the packing motifs, all **DNF–V** derivatives form well-

overlapped core structures. Note that the core structures assemble without molecular displacement in the direction of the molecular longitudinal axis for both **C_{10}–DNF–VV** and **C_{10}–DNF–VW** (Figure 3). Therefore, all **DNF–V** derivatives could exhibit comparable FET performances, reaching a mobility of approximately 1.0 $cm^2 V s^{-1}$, regardless of the substitution positions, as we have already reported.[14,17] From the theoretical calculations of these derivatives, their effective masses, which are inversely proportional to carrier mobility, are analyzed from electronic band structures calculated by PBEPBE/6-31G(d) level with a periodic boundary condition (Supplementary Figures 1–3). Indeed, for all **DNF–V** derivatives, the hole effective masses in the transverse direction ($m_{\perp}^*$) are of similar values, in the range of 1.7–2.5 (Figure 2a). In sharp contrast, their sulfur-bridge counterparts, **DNT–V** derivatives, are susceptible to molecular displacement. Indeed, **C_{10}–DNT–VV**, assembled with a large displacement of 1.27 Å, exhibits rather poor performance in comparison with **C_{10}–DNT–VW**, which forms a well overlapped structure.[13] In view of the distance between the centroids in the core structures, for **C_{10}–DNF–VV**, the distance in the head-to-tail and tail-to-tail molecules is particularly longer than those of the parent **DNF–V** and **C_{10}–DNF–VW** (Supplementary Table 1). This difference is probably due to the presence of alkyl chains attached at the tail positions, namely, 3,10-positions, which inhibit densely packed structure and may affect their fundamental properties. The crystal density of **C_{10}–DNF–VV** (1.058 g cm^{-3}) is, therefore, lower than that of **C_{10}–DNF–VW** (1.081 g cm^{-3}).

Solubility

We tested the solubility of **DNF–V** derivatives in commonly used organic solvents, such as chloroform and toluene, at room temperature and found significant effects of the substitution positions and the length of alkyl side chains (Supplementary Table 2). Surprisingly, a series of **C_n–DNF–VV**s ($n=6$, 8 and 10) derivatives exhibit high solubilities of over 1 wt%, and those with the shorter alkyl chains tend to possess higher solubility. This trend is in good accordance with the case of **Ph–BTBT–C_n**. The solubility of **Ph–BTBT–C_n** rapidly increases with increasing chain length from $n=0$ to 3 and then gradually decreases with longer alkyl chain.[18] Indeed, **C_6–DNF–VV** exhibits a remarkably high solubility (3.2 wt% in chloroform and 2.4 wt% in toluene). In contrast, unsubstituted **DNF–V** and **C_8–** and **C_{10}–DNF–VW** derivatives have solubilities <0.10 wt% in the same condition. The counterpart with shorter alkyl chains, **C_6–DNF–VW**, exhibits improved solubility of 0.16 wt% in toluene at room temperature; however, the solubility is rather low in comparison with **DNF–VV** derivatives. The high solubilities of **C_n–DNF–VV**s might stem from the above-mentioned lower packing density that is related to the position of the alkyl chains and the larger internal dipole moment. The calculated internal dipole moment of **C_{10}–DNF–VV** is as high as 1.47 debye (D), whereas, those of **DNF–V** and **C_{10}–DNF–VW** were of lower values of 0.39 and 0.95 D, respectively.

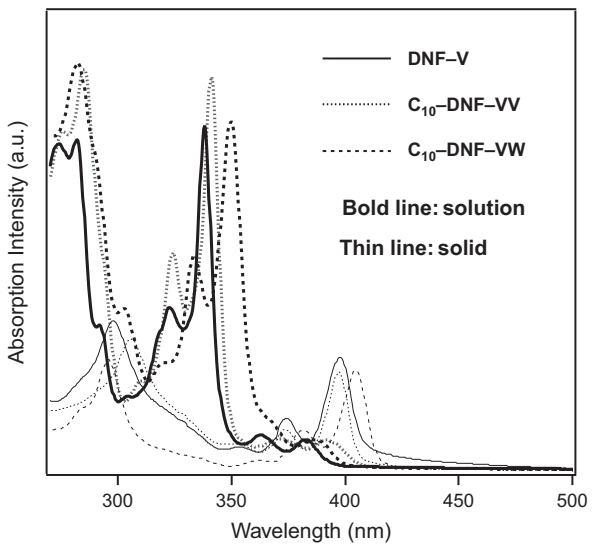

Figure 5 Absorption spectra of **DNF–V**, **C_{10}–DNF–VV**, and **C_{10}–DNF–VW** in 1,2-dichloroethane solution (bold line) and in thin-film form (thin line).

Thermal properties

Chemical stability and structural stability in the crystal phase against heat could demonstrate thermally durable organic electronic devices. First, to ascertain their thermal stabilities, thermogravimetric analysis was performed on alkyl-substituted **DNF–V** derivatives up to 500 °C under nitrogen atmosphere. Indeed, all molecules do not exhibit thermal decomposition; rather, they completely evaporate after melting (Figure 4a and b). The melting points of these compounds were also secured by observation through microscopy. Next, the first phase-transition temperatures from each crystal were measured using DSC, as shown in Figure 4c and d, compared with 2,9-dialkylated pentacenes ($n=6$, 8 and 10). Importantly, alkylated **DNF–V** derivatives exhibit a different trend in comparison with the sulfur-bridged analogs. Notably, **C_{10}–DNF–VV** does not form a liquid crystal phase as a mesophase and thus retains the crystal phase at the high temperature of 176 °C. In contrast, its sulfur-bridged counterpart (**C_{10}–DNT–VV**), which assembles with a large molecular displacement in crystal phase, transforms into the liquid crystal phase at the lower temperature of only 90 °C.[13] In addition, as the length of the alkyl chains shortens, the phase-transition temperatures of **C_n–DNF–VV**s increase up to 199 °C. This tendency indicates that the characteristic of a rigid **DNF–V** core becomes dominant as the alkyl chain shortens. In contrast, **C_n–DNF–VW** showed several crystal-crystal phase-transitions and then transformed to smectic liquid-crystalline states as a distinct feature. For example, the DSC thermogram of **C_6–DNF–VW** shows several small endothermic peaks ranging from 150 to 220 °C and a large endothermic peak at 246 °C (Figure 4d), which corresponds to a crystalline–smectic phase-transition and a subsequent smectic–isotropic liquid phase-transition.[19] During a cooling process from the isotropic liquid phase at a rate of 1 K min^{-1}, these two transition peaks were detected separately, suggesting the formation of the smectic phase from 243.5 to 241.6 °C (Supplementary Figure 4). Indeed, from observations of samples under a polarized optical microscope, the typical focal conic texture of the smectic phases was observed in this narrow temperature range (Supplementary Figure 5). Regarding the DSC traces of **C_8–DNF–VW** and **C_{10}–DNF–VW** during cooling, the first phase transitions were detected as shoulders (Supplementary Figure 4). It is difficult to study the phase transition behavior in such narrow temperature ranges using X-ray diffraction measurements because of the low temperature resolution. Therefore, to further characterize the liquid-crystalline behavior, X-ray diffraction measurements were conducted for **C_6–DNF–VW**. The X-ray diffraction pattern of **C_6–DNF–VW** at 245 °C shows diffraction peaks at 27.7, 13.9, 9.3, 7.0, and 5.6 Å (Supplementary Figure 6a), suggesting the formation of lamellar structures. In the wide-angle region, obvious diffraction peaks were not detected. These results indicate that **C_6–DNF–VW** exhibits a smectic phase with the interlayer distance of 27.8 Å. In the lower temperature region, **C_6–DNF–VW** exhibits several crystalline phases, as confirmed by the X-ray diffraction peaks

Table 1 Summarized optical properties of DNF–V derivatives and DNT–V for comparison

Compounds	λ_{max}^{abs} *(nm) in solution*[a]	λ_{max}^{abs} *(nm) in thin film*[b]	λ_{max}^{em} *(nm) in solution*[c]	Φ_f *(%) in solution*[d]	λ_{max}^{em} *(nm) in solution*[e]	Φ_f *(%) in solid*[f]
DNF–V	322, 337, 362, 382	298, 354, 374, 396	389, 410, 431 (sh)	83	408 (sh), 427, 455, 488, 524	72
DNT–V	327, 343, 383, 404	275, 313, 400, 425	422, 441	8	462	3
C_6–DNF–VV	322, 340, 369, 389	294, 346, 379, 401	398, 419, 444 (sh)	83	411, 432, 453, 489 (sh)	17
C_{10}–DNF–VV	323, 340, 369, 389	296, 363, 381, 404	398, 419, 444 (sh)	87	411, 435, 456 (sh)	18
C_6–DNF–VW	331, 347, 359 (sh), 380	304, 353, 372, 394	389, 409, 431 (sh)	89	404 (sh), 422, 445	51
C_{10}–DNF–VW	331, 348, 359 (sh), 381	306, 353, 374, 397	388, 409, 431 (sh)	83	407 (sh), 424, 448	40

[a]Absorption spectra measured in 1,2-dichloroethane at room temperature. sh: shoulder.
[b]Absorption spectra measured in vacuum deposited thin film on quarts substrate at room temperature.
[c]Emission spectra excited at 340 nm measured in 1,2-dichloroethane at room temperature. sh: shoulder.
[d]Fluorescence quantum yield in solution.
[e]Emission spectra excited at 340 nm measured in solid state. sh: shoulder.
[f]Fluorescence quantum yield in solid.

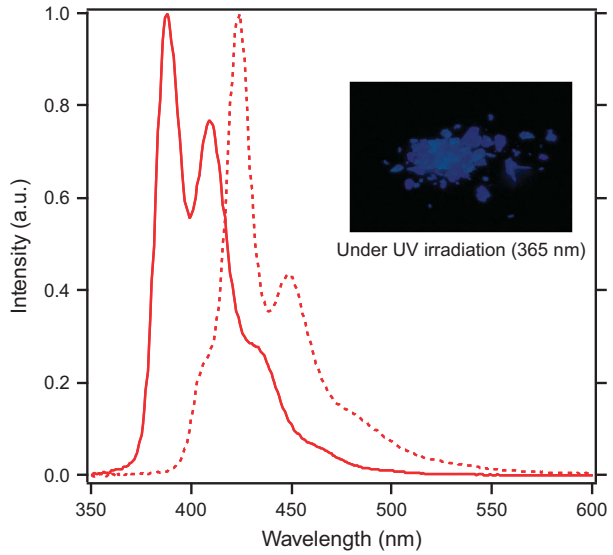

Figure 6 Fluorescence spectra and photographs (inset) of **C_{10}–DNF–VW** (solid line: 1,2-dichloroethane solution, dotted line: solid).

in the wide-angle region (Supplementary Figure 6b) and the loss of macroscopic fluidity. The first phase-transition temperatures (128–150 °C) of **C_n–DNF–VW**s observed during the heating process are still higher than those of the pentacene derivatives, as summarized in Supplementary Table 3. 2,9-Dialkylated pentacenes ($n=6$, 8 and 10) transform into the smectic phase in the temperature range of 89–105 °C,[6] at which the rod-type pentacene core are rotating along its molecular longitudinal axis in a lamellar mesophase. We thus conjectured that the bent-type **DNF–V** core could suppress the molecular spin motion, resulting in the higher phase-transition temperature. Here, we found that the phase-transition temperatures increase in the order of 2,9-dialkylated pentacenes, **C_n–DNF–VW**s, and **C_n–DNF–VV**s. The different phase-transition behaviors between **C_n–DNF–VV**s and **C_n–DNF–VW**s might stem from the molecular shape resulting from the presence of the alkyl chains. **C_n–DNF–VV**s with the alkyl chains at the 2,10-positions have an overall banana-shaped structure, which completely inhibits the liquid crystal phase from forming. Overall, **C_n–DNF–VV**s simultaneously achieve high solubility and high structural stability in the crystal phase.

Photophysical property

The photophysical properties of the oxygen-bridged V-shaped compounds were examined by absorption and emission spectral measurements. Figure 5 shows the absorption spectra of **DNF–V** derivatives in 1,2-dichloroethane solutions. The longest absorption maximum is located in the range of 380–390 nm, suggesting their large HOMO–LUMO gaps of over 3.0 eV. Indeed, the longest absorption maximum wavelengths of **DNF–V** derivatives are shorter than those of **DNT–V**s (*c.f.* **DNT–V**: 404 nm) because the oxygen atom, with a high electronegativity, suppresses π-electron conjugation in its core structure. In the thin film form of the material prepared by vacuum deposition technique, each compound exhibited red-shifted absorption characteristics in comparison with those in solution. The spectral data are summarized in Table 1. We next measured the fluorescence spectra and quantum yields (Φ_f) of the **DNF–V** derivatives. **DNF–V** derivatives showed deep-blue emissions because of the large HOMO–LUMO gap, as estimated from the absorption spectra. Representative fluorescence spectra and an emission photograph of **C_{10}–DNF–VW** are shown in Figure 6. The fluorescence quantum yields in 1,2-dichloroethane solution were very high, in the range of 83–89%, despite the presence of alkyl chains, whereas the sulfur bridged congeners, **DNT–V**s, show a quite low quantum yield of less than 10%, primarily because of the strong spin-orbital coupling by the sulfur atom. In the solid state, different fluorescent features were observed among the **DNF–V** derivatives. Although the unsubstituted **DNF–V** exhibited a very high Φ_f of 72% in the solid state, alkylated **DNF–V** exhibited a value in the range of 15–51%, depending on the length and position of the alkyl chains. Alkylated **DNF–VW** exhibited relatively high values of Φ_f of 51% for **C_6–DNF–VW** and 40% for and **C_{10}–DNF–VW**, respectively. In comparison, the quantum yields of **C_n–DNF–VV**s are only 17–18%. To understand the origin of this trend, we also measured the fluorescence lifetimes (τ). These values together with the quantum yields (Φ_f) are used to calculate the radiative (k_f) and non-radiative relaxation (k_{nr}) rate constants from the singlet excited states according to the following formulas: $k_f=\Phi_f/\tau$ and $k_{nr}=(1-\Phi_f)/\tau$. The results are summarized in

Table 2 Fluorescence lifetime and radiative and non-radiative rate constants of the DNF–V derivatives

	Solution			*Solid*		
Compounds	τ *(ns)*	$k_f(10^7\ s^{-1})$	$k_{nr}\ (10^7\ s^{-1})$	τ *(ns)*	$k_f(10^7\ s^{-1})$	$k_{nr}(10^7\ s^{-1})$
DNF–V	23.1	3.60	0.74	17.4	4.13	1.61
C_6–DNF–VW	22.3	3.98	0.49	14.8	3.44	3.31
C_{10}–DNF–VW	22.7	3.66	0.75	9.11	4.39	6.58
C_6–DNF–VV	22.8	3.63	0.74	8.06	2.11	10.3
C_{10}–DNF–VV	22.6	3.85	0.58	5.89	3.06	13.9

Table 2. In solution, both k_f and k_{nr} are comparable for all compounds, suggesting that their electronic states are similar among them. In contrast, in the solid state, whereas the k_f of **C_n–DNF–VW**s and **C_n–DNF–VV**s ($n = 6$, 10) are comparable to one another for all the compounds ($2.11–3.44 \times 10^7$ s^{-1}), the k_{nr} values of the more emissive **C_n–DNF–VW**s (3.31×10^7 s^{-1} for **C_6** and 6.58×10^7 s^{-1} for **C_{10}**) are much smaller than those of **C_n–DNF–VV**s (10.3×10^7 s^{-1} for **C_6** and 13.9×10^7 s^{-1} for **C_{10}**). The differences in the non-radiative rate constants might be ascribed to the distortion angle against the π-planes, as revealed by X-ray single crystal analyzes. The smaller distortion angles of **C_n–DNF–VW**s than those of **C_n–DNF–VV**s therefore suppress thermal deactivation via structural changes in the solid state. Likewise, as the flexible alkyl chains shorten, the k_{nr} values become smaller.

In conclusion, we systematically investigated alkylated **DNF–VV** and **DNF–VW** derivatives and elucidated the impacts of the substitution position and the length of alkyl side chains on their physicochemical properties based on their packing structures. All **DNF–V** derivatives form the herringbone packing motif, and their molecular geometries and the distance between centroids both rely on the substitution position of the alkyl chains. For both alkylated **DNF–VV** and **DNF–VW** derivatives, both the solubilities and the phase-transition temperatures increase with shorter attached alkyl chains. In particular, alkylated **DNF–VV** simultaneously achieves a high solubility of over 1 wt% and a high thermal stability in the crystal phase for temperatures of up to 199 °C. This observed trend promotes the production of semiconductor materials with solution-processability and thermal durability. In addition, alkylated **DNF–VW** exhibits a higher value of Φ_f of up to 51% in the solid state compared to **C_n–DNF–VV**s, probably because of the planar geometry in the crystal phase. The results of this systematic investigation provide us with a rational molecular design for the development of practical organic semiconducting materials. Application to the synthesized derivative is now ongoing in our laboratory.

CONFLICT OF INTEREST

The authors declare no conflict of interest.

ACKNOWLEDGEMENTS

This work was supported by JST PRESTO program '*Molecular Technology and Creation of New Functions*' and KAKENHI. CM thanks the JSPS Grant-in-Aid for Young Scientists (B) (No. 25810118). TO also thanks the JSPS Grant-in-Aid for Scientific Research (B) (No. 25288091). MY thanks the JSPS Grant-in-Aid for Scientific Research (C) (No. 26410254) and the Kansai University Subsidy for Supporting Young Scholars, 2014. MH thanks the Supported Program for the Strategic Research Foundation at Private Universities. The authors thank the Comprehensive Analysis Center (CAC), the Institute of Scientific and Industrial Research (ISIR), Osaka Univ. for the elemental analysis measurements.

1 Bao, Z. & Locklin, J. *Organic Field-Effect Transistors* 1st ed (CRC Press, Florida, 2007).
2 Baude, P. F., Ender, D. A., Haase, M. A., Kelley, T. W., Muyres, D. V. & Theiss, S. D. Pentacene-based radio-frequency identification circuitry. *Appl. Phys. Lett.* **82**, 3964–3966 (2003).
3 Steudel, S., Myny, K., Arkhipov, V., Deibel, C., Vusser, S. D., Genoe, J. & Heremans, P. 50 MHz rectifier based on an organic diode. *Nat. Mater.* **4**, 597–600 (2005).
4 Lin, Y. Y., Gundlach, D. J., Nelson, S. F. & Jackson, T. N. Stacked pentacene layer organic thin-film transistors with improved characteristics. *IEEE Electron Dev. Lett.* **18**, 606–608 (1997).
5 Anthony, J. E., Brooks, J. S., Eaton, D. L. & Parkin, S. R. Functionalized pentacene: Improved electronic properties from control of solid-state order. *J. Am. Chem. Soc.* **123**, 9482–9483 (2001).
6 Okamoto, K., Kawamura, T., Sone, M. & Ogino, K. Study on liquid crystallinity in 2,9-dialkylpentacenes. *Liq. Cryst.* **34**, 1001–1007 (2007).
7 Maliakal, A., Raghavachari, K., Katz, H., Chandross, E. & Siegrist, T. Photochemical stability of pentacene and a substituted pentacene in solution and in thin films. *Chem. Mater.* **16**, 4980–4986 (2004).
8 Sakanoue, T. & Sirringhaus, H. Band-like temperature dependence of mobility in a solution-processed organic semiconductor. *Nat. Mater.* **9**, 736–740 (2010).
9 Giri, G., Verploegen, E., Mannsfeld, S. C. B., Atahan-Evrenk, S., Kim, D. H., Lee, S. Y., Becerril, H. A., Aspuru-Guzik, A., Toney, M. F. & Bao, Z. Tuning charge transport in solution-sheared organic semiconductors using lattice strain. *Nature* **480**, 504–508 (2011).
10 Chen, J., Anthony, J. & Martin, D. C. Thermally induced solid-state phase transition of bis(triisopropylsilylethynyl)pentacene crystals. *J. Phys. Chem. B* **110**, 16397–16403 (2006).
11 Ebata, H., Izawa, T., Miyazaki, E., Takimiya, K., Ikeda, M., Kuwabara, H. & Yui, T. Highly soluble [1]benzothieno[3,2-b]benzothiophene (BTBT) derivatives for high-performance, solution-processed organic field-effect transistors. *J. Am. Chem. Soc.* **129**, 15732–15733 (2007).
12 Kang, M. J., Doi, I., Mori, H., Miyazaki, E., Takimiya, K., Ikeda, M. & Kuwabara, H. Alkylated dinaphtho[2,3-b:2',3'-f]thieno[3,2-b]thiophenes (Cn-DNTTs): Organic semiconductors for high-performance thin-film transistors. *Adv. Mater.* **23**, 1222–1225 (2011).
13 Okamoto, T., Mitsui, C., Yamagishi, M., Nakahara, K., Soeda, J., Hirose, Y., Miwa, K., Sato, H., Yamano, A., Matsushita, T., Uemura, T. & Takeya, J. V-shaped organic semiconductors with solution processability, high mobility, and high thermal durability. *Adv. Mater.* **25**, 6392–6397 (2013).
14 Nakahara, K., Mitsui, C., Okamoto, T., Yamagishi, M., Matsui, H., Ueno, T., Tanaka, Y., Yano, M., Matsushita, T., Soeda, J., Hirose, Y., Sato, H., Yamano, A. & Takeya, J. Furan fused V-shaped organic semiconducting materials with high emission and high mobility. *Chem. Commun.* **50**, 5342–5344 (2014).
15 Cicoira, F. & Santato, C. Organic light emitting field effect transistors: Advances and perspectives. *Adv. Funct. Mater.* **17**, 3421–3434 (2007).
16 Arienti, A., Bigi, F., Maggi, R., Moggi, P., Rasyelli, M., Sartori, G. & Trerè, A. Highly selective conversion of hydroxylated biaryls to dibenzofuran derivatives over zeolite catalyst. *J. Chem. Soc. Perkin Trans.* **1**, 1391–1394 (1997).
17 Mitsui, C., Tanaka, Y., Tanaka, S., Yamagishi, M., Nakahara, K., Yano, M., Sato, H., Yamano, A., Matsui, H., Takeya, J. & Okamoto, T. High performance oxygen-bridged N-shaped semiconductors with a stabilized crystal phase and blue luminescence. *RSC Adv.* **6**, 28966–28969 (2016).
18 Inoue, S., Minemawari, H., Tsutsumi, J., Chikamatsu, M., Yamada, T., Horiuchi, S., Tanaka, M, Kumai, R., Yoneya, M. & Hasegawa, T. Effects of substituted alkyl chain length on solution-processable layered organic semiconductor crystals. *Chem. Mater.* **27**, 3809–3812 (2016).
19 Funahashi, M. Development of liquid-crystalline semiconductors with high carrier mobilities and their application to thin-film transistors. *Polym. J.* **41**, 459–469 (2009).

Supplementary Information accompanies the paper on Polymer Journal website (http://www.nature.com/pj)